Cross sections and polarization fractions for elastic e^--O_2 collisions

L. E. Machado and E. M. S. Ribeiro
Departamento de Física, Universidade Federal de São Carlos, 13565-905 São Carlos, SP, Brazil

M.-T. Lee and M. M. Fujimoto
Departamento de Química, Universidade Federal de São Carlos, 13565-905 São Carlos, SP, Brazil

L. M. Brescansin
Instituto de Física Gleb Wataghin, Universidade Estadual de Campinas, 13083-970 Campinas, SP, Brazil
(Received 4 February 1999; revised manuscript received 30 March 1999)

The Schwinger variational iterative method and the distorted-wave approximation are combined to study elastic electron scattering by O_2 for incident energies ranging from 5 to 500 eV. Differential, integral, and momentum transfer cross sections as well as polarization fractions are reported. A complex optical potential, which accounts for the static, exchange, correlation-polarization, and absorption contributions is used to describe the electron-molecule interaction. Comparison of our calculated results with experimental and other theoretical results is encouraging. [S1050-2947(99)08508-X]

I. INTRODUCTION

Molecular oxygen plays a fundamental role in the physics and chemistry of earth's atmosphere. For example, electron-impact cross sections for some excitation processes in O_2 are very important for studies of auroras [1]. They are also useful in understanding other processes that take place in the ionosphere. This has motivated several experimental and theoretical investigations on e^--O_2 collisions in the past.

Some early measurements of elastic differential and integral cross sections for low-energy electron scattering by O_2 molecules were performed by Trajmar *et al.* [1] and by Shyn and Sharp [2]. For incident energies above 100 eV, elastic e^--O_2 scattering was also studied by Iga *et al.* [3], Bromberg [4], and Daimon *et al.* [5]. A review of results prior to 1989 was reported by Itikawa *et al.* [6]. Also, elastic integral and grand total (elastic plus inelastic) cross sections for e^--O_2 scattering have been critically reviewed and ''recommended'' by Kanik *et al.* [7] in the (1–1000)-eV energy range. Recently, differential and integral cross sections for elastic scattering of low-energy electrons by O_2 were reported by Wöste *et al.* [8] and Sullivan *et al.* [9].

On the theoretical side, da Paixão *et al.* [10] used the Schwinger multichannel method (SMC) for the determination of elastic differential cross sections (DCSs) at incident energies of 10 and 15 eV. In their calculations three low-lying electronic states ($X\,^3\Sigma_g^-$, $a\,^1\Delta_g$, and $b\,^1\Sigma_g^+$) were included. Noble and Burke [11] reported a nine-state R-matrix calculation of integral cross sections (ICSs) for elastic scattering of electrons by molecular oxygen. The same R-matrix method has been applied recently by Fullerton *et al.* [12], Nordbeck *et al.* [13], and Wöste *et al.* [8] to calculate elastic DCSs and ICSs for some selected energies in the (4–15)-eV energy range. Those calculated DCSs are in general good agreement with the available experimental data for incident energies above 10 eV. Nevertheless, at 10 eV and below, the calculated results were unable to reproduce the measured data, particularly at small scattering angles. Moreover, there

is a lack of results for cross sections for energies above 15 eV.

Since O_2 is an open-shell system, depolarization can be observed during the collision of low-energy polarized electrons with this molecule, influenced by spin-exchange effects. Recently, an increasing number of experiments with polarized electron beams have been done. Using spin-polarized electrons, Ratliff *et al.* [14] have made measurements of the polarization fraction P'/P (the ratio between final and initial polarization of the electronic beam) for both e^--NO and e^--O_2 collisions at thermal energies. Hegemann *et al.* [15] and Hegemann [16] have measured the ratio P'/P for the elastic scattering of polarized electrons by unpolarized NO ($X\,^2\Pi$) and O_2 ($X\,^3\Sigma_g^-$) targets at energies up to 15 eV. These authors noticed that spin-exchange effects in molecular scattering are considerably smaller than the corresponding ones for atomic targets. da Paixão *et al.* [10] have calculated P'/P for elastic electron scattering by O_2 molecules at energies of 10 and 15 eV. Their study has shown that the small P'/P ratios observed for molecular systems are due to the averaging over the molecular orientations. Fullerton *et al.* [12] also calculated P'/P for electrons elastically scattered by randomly oriented O_2 targets for incident energies ranging from 0.25 to 15 eV and confirmed the findings of da Paixão *et al.* [10]. Finally, Nordbeck *et al.* [13] and Wöste *et al.* [17] reported some new results of P'/P for this molecule. Their results show a correlation between the occurrence of structures in P'/P and the minima of the DCSs at some scattering angles.

In this work, we combine the Schwinger variational iterative method [18] (SVIM) and the distorted-wave approximation [19] (DWA) to study the electron scattering by an oxygen molecule in a wide energy range. In particular, we report elastic DCSs in the (5–500)-eV energy range, as well as the P'/P ratios in the (5–50)-eV range. To describe the electron-molecule interaction, we use a complex optical interaction potential, which accounts for the static, exchange, correlation-polarization, and absorption contributions and is

derived from a fully molecular near-Hartree-Fock self-consistent-field (SCF) wave function. This theoretical model has been applied recently by Lee and Iga [20] for the elastic electron scattering by N_2 in the (20–800)-eV range. In their study, the comparison between calculated and measured cross sections was very encouraging. Therefore, the same model could be expected to be suitable to describe e^--O_2 elastic collisions.

The organization of the paper is the following. In Sec. II we will present a brief discussion of the theory used. The details of the calculations will be discussed in Sec. III. The comparison with previous theoretical and experimental results will be presented in Sec. IV, where we also summarize our conclusions.

II. THEORY

Since the details of the SVIM and DWA have already been presented in previous works [18,21], only a brief outline of the theory will be given here. In a j_t-basis representation [22], the laboratory-frame (LF) elastic DCSs, averaged over the molecular orientations, are given by

$$\frac{d\sigma}{d\Omega} = \sum_{j_t m_t m_t'} \frac{1}{(2j_t+1)} |B_{m_t m_t'}^{j_t}(\hat{k}')|^2, \tag{1}$$

where $\vec{j}_t = \vec{l}' - \vec{l}$ is the angular momentum transferred during the collision, m_t' and m_t are the projections of $\vec{j}_t$ along the laboratory and molecular axes, respectively, and $\hat{k}'$ is the scattering solid angle in the LF. In Eq. (1), $B_{m_t m_t'}^{j_t}$ is the coefficient of the j_t-basis expansion of the LF-scattering amplitude which is given by

$$B_{m_t m_t'}^{j_t}(\hat{k}') = \sum_{ll'm} (-1)^m a_{ll'm}(ll'0m_t|j_t m_t)$$
$$\times (ll'mm'|j_t m_t') Y_{lm_l}(\hat{k}'), \tag{2}$$

where the dynamical coefficients $a_{ll'mm'}$ can be written in terms of partial-wave components of the electronic portion of the body-frame fixed-nuclei transition T-matrix elements as

$$a_{ll'm} = -(1/2)\pi[4\pi(2l'+1)]^{(1/2)}i^{l'-l}\langle lm|T|l'm\rangle. \tag{3}$$

The elastic scattering transition T matrix is calculated using a complex optical potential, given by

$$V_{opt} = V^{SEP} + iV_{ab}, \tag{4}$$

where V^{SEP} is the real part of the interaction potential formed by the static, the exchange, and the correlation-polarization contributions as

$$V^{SEP} = V_{st} + V_{ex} + V_{CP}, \tag{5}$$

and V_{ab} is the absorption potential. In our calculation, V_{st} and V_{ex} are treated exactly, while V_{CP} is obtained in the framework of the free-electron-gas model derived from a parameter-free local density, as prescribed by Padial and Norcross [23]. The dipole polarizabilities $\alpha_0 = 10.74$ a.u.

and $\alpha_2 = 4.93$ a.u. [24] were assumed to calculate the asymptotic form of V_{CP}. The absorption potential V_{ab} in Eq. (4) is given by [25]

$$V_{ab}(\vec{r}) = -\rho(\vec{r})(T_L/2)^{1/2}(8\pi/5k^2 k_F^3)H(\alpha+\beta-k_F^2)$$
$$\times (A+B+C), \tag{6}$$

where

$$T_L = k^2 - V^{SEP}, \tag{7}$$

$$A = 5k_F^3/(\alpha-k_F^2), \tag{8}$$

$$B = -k_F^3[5(k^2-\beta)+2k_F^2]/(k^2-\beta)^2, \tag{9}$$

and

$$C = 2H(\alpha+\beta-k^2)\frac{(\alpha+\beta-k^2)^{5/2}}{(k^2-\beta)^2}. \tag{10}$$

In Eqs. (6)–(10), k^2 is the energy (in rydbergs) of the incident electron, k_F is the Fermi momentum, and $\rho(\vec{r})$ is the local electronic density of the target. $H(x)$ is a Heaviside function defined by $H(x)=1$ for $x \geq 0$ and $H(x)=0$ for $x<0$. According to version 3 of the quasi-free-scattering model of Staszewska et al. [25],

$$\alpha(\vec{r},E) = k_F^2 + 2(2\Delta-I) - V^{SEP} \tag{11}$$

and

$$\beta(\vec{r},E) = k_F^2 + 2(I-\Delta) - V^{SEP}, \tag{12}$$

where Δ is the average excitation energy and I is the ionization potential. In this study, the published values $I = 12.07$ eV and $\Delta = 21.20$ eV [26] are used in the calculations.

In the two-potential formalism the transition T matrix can be written as

$$T_{fi} = \langle \Phi_f | U_1 | \chi_i^+ \rangle + \langle \chi_f^- | U_2 | \Psi_i^+ \rangle, \tag{13}$$

where the superscripts $(+)$ and $(-)$ designate the outgoing-wave and incoming-wave boundary conditions, respectively, and Ψ, χ, and Φ are solutions of the corresponding Schrödinger equations:

$$(H_0 + U - E)\Psi = 0, \tag{14}$$

$$(H_0 + U_1 - E)\chi = 0, \tag{15}$$

and

$$(H_0 - E)\Phi = 0, \tag{16}$$

where $H_0 = -\frac{1}{2}\nabla^2$ is the unperturbed Hamiltonian operator for a free electron and U is the interaction potential that can be arbitrarily split as

$$U = U_1 + U_2. \tag{17}$$

In the present study, U_1 is taken as the real part of the complex optical potential, whereas U_2 is the imaginary ab-
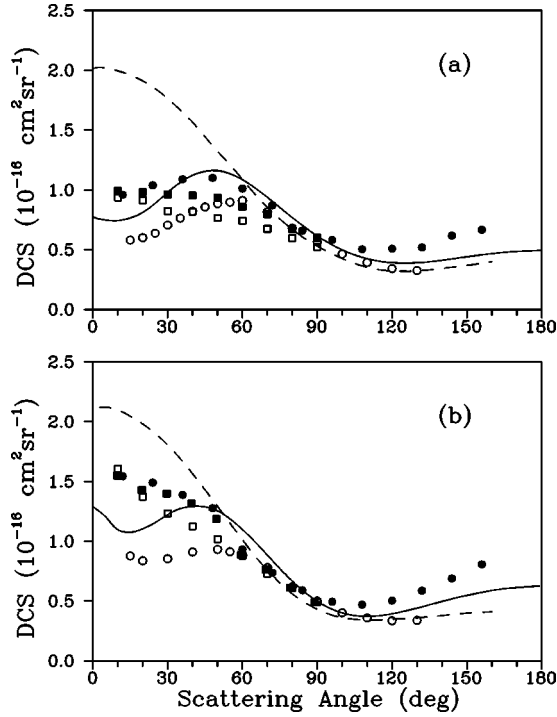
FIG. 1. DCSs for elastic e^--O_2 scattering at an impact energy of (a) 5 eV and (b) 7 eV. Solid line, present results; dashed line, theoretical results of Wöste *et al.* [8]; experimental results are of Shyn and Sharp [2] (closed circles); Sullivan *et al.* [9] (closed circles); Wöste *et al.* [8] (full squares); Trajmar *et al.* [1] (open squares).

sorption potential. The corresponding distorted-wave scattering equation (15) is solved using the SVIM (Ref. [18]). Furthermore, a distorted-wave approximation is used to calculate the absorption part of the T matrix:

$$T_{ab} = i \langle \chi_f^- | V_{ab} | \chi_i^+ \rangle. \tag{18}$$
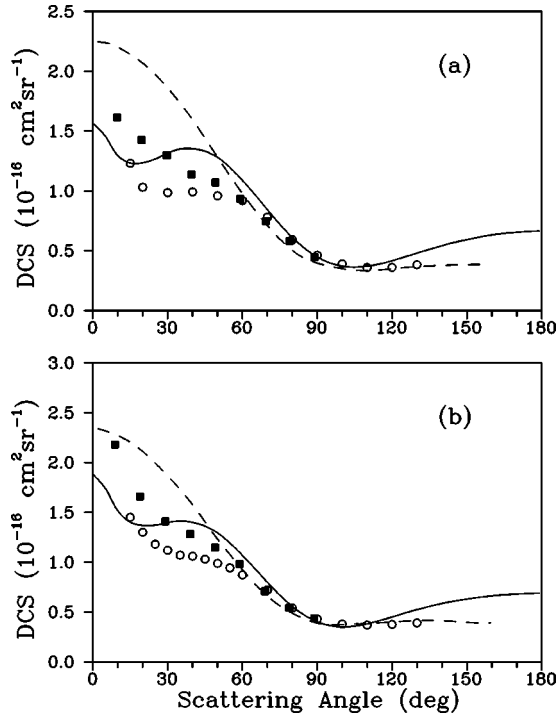

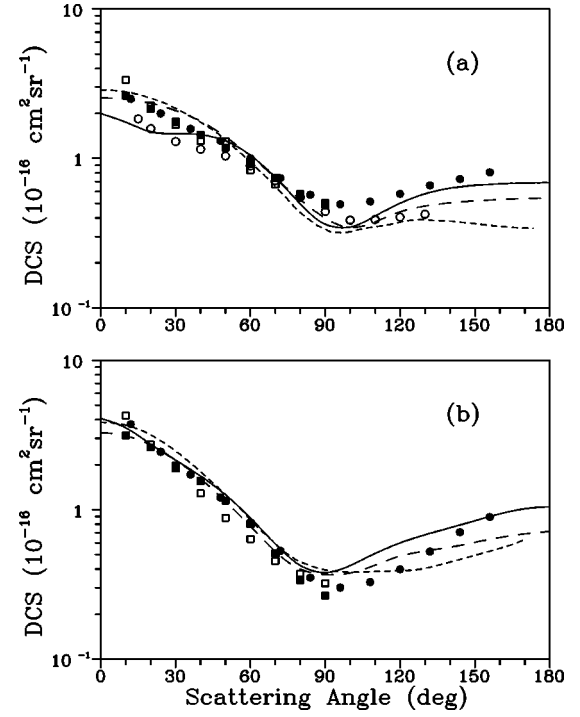FIG. 2. Same as Fig. 1, but for (a) 8 eV and (b) 9 eV.

FIG. 3. Same as Fig. 1, but for (a) 10 eV and (b) 15 eV. The symbols are the same as in Fig. 1, except: short-dashed line, theoretical results of da Paixão *et al.* [10].

In SVIM calculations, it is convenient to transform the Schrödinger equation (15) into an integral form
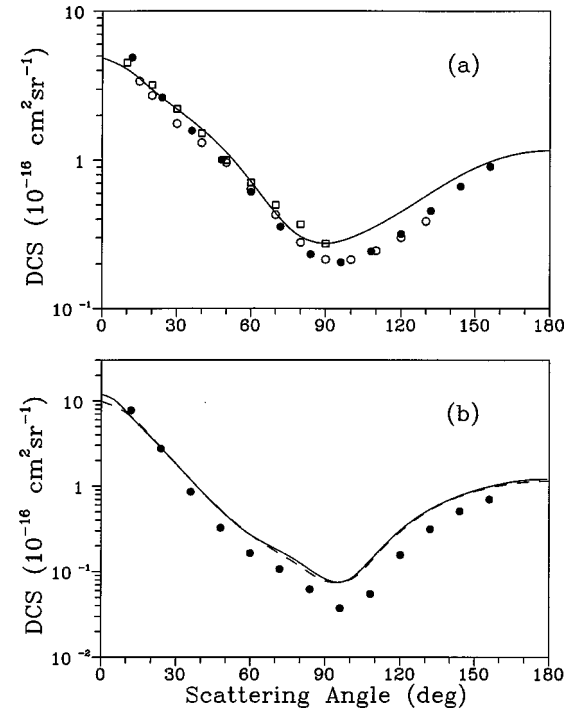
$$\chi^P = \Phi + G_0^P U_1 \chi^P \tag{19}$$

FIG. 4. Same as Fig. 1, but for (a) 20 eV and (b) 50 eV. The symbols are the same as in Fig. 3, except in (b): solid line, present DCSs calculated with absorption effects; dashed line, present DCSs without absorption effects.
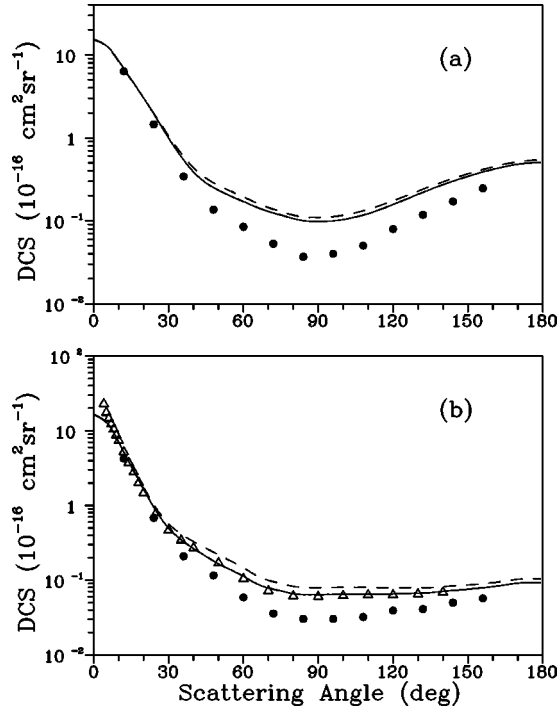
FIG. 5. Same as Fig. 1, but for (a) 100 eV and (b) 200 eV. The symbols are the same as in Fig. 4(b), except: experimental results are of Shyn and Sharp [2] (closed circles); Daimon et al. [5] (open triangles).

or into its partial-wave expanded form

$$\chi_{klm}^{P} = \Phi_{klm} + G_0^P U_1 \chi_{klm}^P , \qquad (20)$$

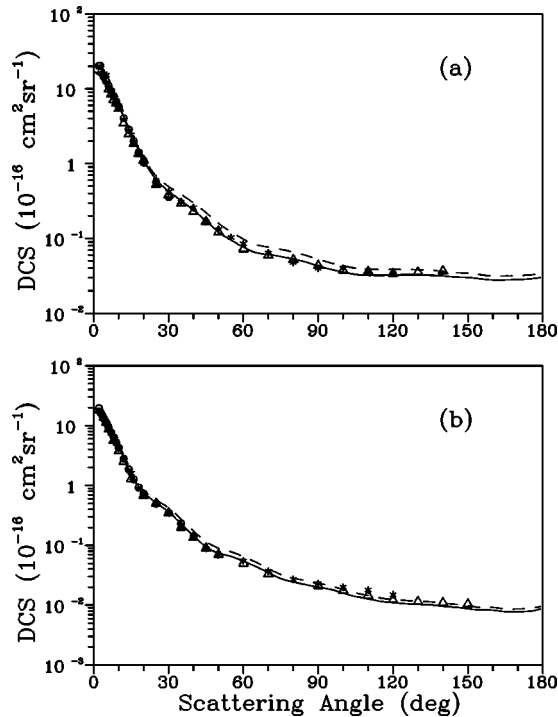where G_0 is the free-particle Green's operator and the superscript P stands for principal value.-

FIG. 6. Same as Fig. 5, but for (a) 300 eV and (b) 500 eV. Experimental results are of Daimon et al. [5] (open triangles); Iga et al. [3] (asterisks); Bromberg [4] (half-filled circles).

TABLE I. DCSs, ICSs, and MTCSs (in 10^{-16} cm^2) for elastic e^--O_2 scattering in the (5–15)-eV range.

Angle (deg)	E_0 (eV)					
	5	7	8	9	10	15
0	0.773	1.288	1.564	1.880	1.995	4.064
10	0.743	1.096	1.294	1.515	1.746	3.526
20	0.811	1.103	1.235	1.368	1.507	2.738
30	0.979	1.222	1.315	1.397	1.461	2.143
40	1.122	1.291	1.353	1.399	1.441	1.678
50	1.161	1.254	1.280	1.294	1.309	1.258
60	1.085	1.098	1.087	1.068	1.050	0.878
70	0.938	0.884	0.843	0.797	0.746	0.589
80	0.768	0.667	0.611	0.556	0.496	0.423
90	0.615	0.498	0.447	0.402	0.362	0.379
100	0.498	0.401	0.371	0.352	0.347	0.423
110	0.424	0.372	0.370	0.381	0.411	0.509
120	0.391	0.393	0.416	0.450	0.501	0.599
130	0.390	0.441	0.479	0.524	0.579	0.679
140	0.411	0.496	0.541	0.585	0.631	0.756
150	0.440	0.547	0.592	0.629	0.660	0.843
160	0.467	0.588	0.632	0.662	0.676	0.937
170	0.485	0.613	0.654	0.680	0.684	1.014
180	0.492	0.624	0.665	0.690	0.688	1.046
ICS	8.744	9.058	9.197	9.338	9.513	11.18
MTCS	6.953	7.021	7.106	7.216	7.379	8.429

TABLE II. DCSs, ICSs, and MTCSs (in 10^{-16} cm^2) for elastic e^--O_2 scattering in the (20–500)-eV range.

Angle (deg)	E_0 (eV)					
	20	50	100	200	300	500
0	4.855	11.87	15.34	16.34	16.85	17.06
10	4.075	7.561	8.406	7.003	6.003	4.559
20	2.978	3.747	3.014	1.634	1.107	0.760
30	2.196	1.827	0.991	0.495	0.427	0.361
40	1.619	0.892	0.386	0.264	0.238	0.143
50	1.127	0.464	0.233	0.165	0.122	0.074
60	0.717	0.210	0.170	0.113	0.076	0.054
70	0.440	0.186	0.129	0.078	0.061	0.035
80	0.305	0.126	0.106	0.065	0.053	0.024
90	0.275	0.082	0.098	0.064	0.043	0.020
100	0.301	0.082	0.103	0.065	0.036	0.016
110	0.360	0.157	0.122	0.065	0.032	0.013
120	0.449	0.305	0.157	0.065	0.032	0.011
130	0.574	0.494	0.208	0.067	0.032	0.010
140	0.726	0.694	0.272	0.071	0.031	0.010
150	0.886	0.885	0.343	0.075	0.030	0.009
160	1.027	1.046	0.417	0.082	0.028	0.008
170	1.124	1.169	0.479	0.091	0.028	0.008
180	1.158	1.204	0.507	0.093	0.030	0.009
ICS	10.26	8.193	5.737	3.583	2.824	2.078
MTCS	7.390	5.290	2.673	1.043	0.604	0.293

We first solve the Lippmann-Schwinger equation [Eq. (19) or Eq. (20)], by assuming an appropriate separable form for the scattering potential U_1:

$$U_1(\vec{r},\vec{r}') \approx U_1^s(\vec{r},\vec{r}') = \sum_{i,j}^{M} \langle \vec{r}|U_1|\alpha_i\rangle (U_1^{-1})_{ij}\langle \alpha_j|U_1|\vec{r}'\rangle,$$
(21)

where U_1^{-1} is the inverse of the matrix with elements $(U_1)_{ij} = \langle \alpha_i|U_1|\alpha_j\rangle$ and $\{\alpha_i\}$ is a set of square integrable basis functions, adequately chosen to represent the separable potential. With this approximation, the partial-wave K-matrix elements can be obtained as

$$K_{ll'm} = \sum_{i,j}^{M} \langle \Phi_{klm}|U_1|\alpha_i\rangle [D^{-1}]_{i,j}\langle \alpha_j|U_1|\Phi_{kl'm}\rangle,$$
(22)

and the corresponding approximate scattering solution with outgoing-wave boundary condition as

$$\chi_{k,lm}^{(+)(S_0)}(\vec{r}) = \Phi_{k,lm}(\vec{r}) + \sum_{i,j=1}^{M} \langle \vec{r}|G_0^{(+)}U_1|\alpha_i\rangle$$
$$\times [D^{(+)^{-1}}]_{ij}\langle \alpha_j|U|\Phi_{k,lm}\rangle.$$
(23)

In Eqs. (22) and (23), D_{ij} is a matrix element defined as

$$D_{ij} = \langle \alpha_i|U_1 - U_1 G^P U_1|\alpha_j\rangle.$$
(24)

Converged scattering wave functions can be obtained through an iterative procedure. For this, a new basis set is formed by augmenting $\{\alpha_i\}$ by a set of new functions

$$S_0 = \{\chi_{kl_1m}^{S_0}, \chi_{kl_2m}^{S_0}, \ldots, \chi_{kl_pm}^{S_0}\},$$
(25)

which are the scattering solutions of Eq. (19). Using this augmented set of functions, a second set of scattering solutions

$$S_1 = \{\chi_{kl_1m}^{S_1}, \chi_{kl_2m}^{S_1}, \ldots, \chi_{kl_pm}^{S_1}\}$$
(26)

is obtained through Eqs. (19)–(23). This iterative procedure is continued until the desired convergence is achieved. It can be shown [27] that the converged wave functions correspond to the exact solutions of the Lippmann-Schwinger equation for the assumed potential U_1.

Since the ground state of O_2 is $X\,^3\Sigma_g^-$, two spin-specific scattering channels, the doublet and the quartet, have to be considered in the present study. Therefore the statistical average of the elastic scattering DCSs is written as

$$\left(\frac{d\sigma}{d\Omega}\right) = \frac{1}{6}\{4|f^{(4)}|^2 + 2|f^{(2)}|^2\},$$
(27)

where $f^{(2)}$ and $f^{(4)}$ are the scattering amplitudes for the doublet and quartet channels, respectively. The spin-flip DCS, $(d\sigma/d\Omega)^{SF}$ can also be expressed in a similar manner as

$$\left(\frac{d\sigma}{d\Omega}\right)^{SF} = \frac{4}{27}|f^{(4)} - f^{(2)}|^2.$$
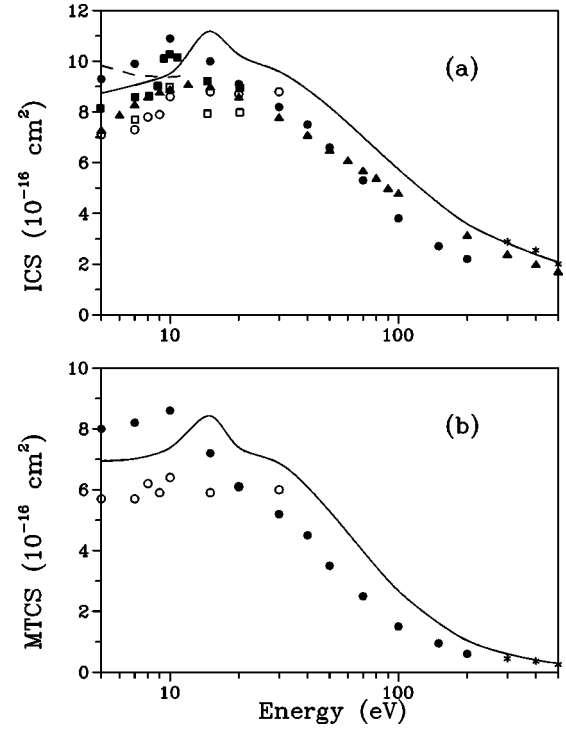(28)

FIG. 7. (a) ICSs and (b) MTCSs for elastic e^--O_2 scattering. Solid line, present calculated results; dashed line, theoretical results of Wöste et al. [8]; experimental results are of Shyn and Sharp [2] (closed circles); Sullivan et al. [9] (open circles); Wöste et al. [8] (closed squares); Trajmar et al. [1] (open squares); Iga et al. [3] (asterisks); Kanik et al. [7] (full triangles).
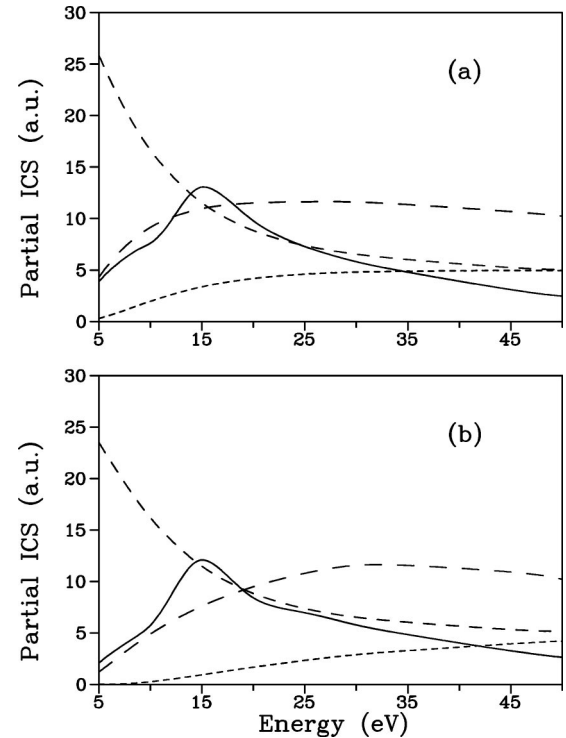

FIG. 8. Present partial-channel ICSs for (a) doublet and (b) quartet couplings. Solid line, Σ_u^- channel; dashed line, Σ_g^- channel; short-dashed line, Π_g channel; long-dashed line, Π_u channel.
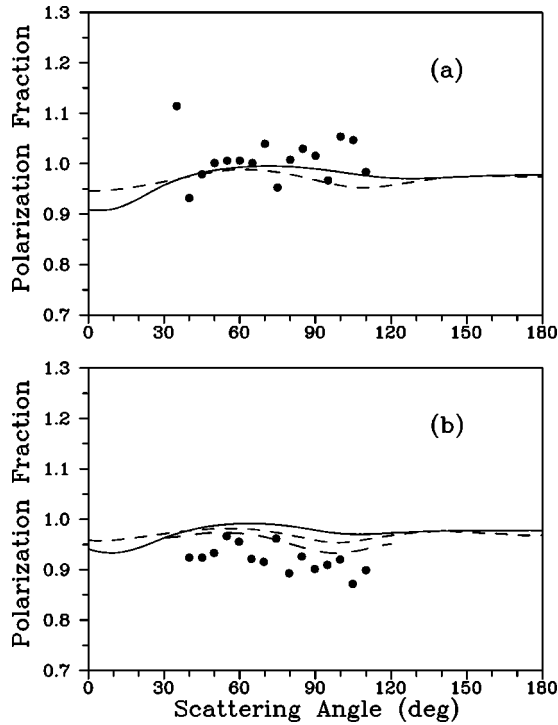
FIG. 9. Polarization fractions for randomly oriented target at an impact energy of (a) 5 eV and (b) 8 eV. Solid line, present results; dashed line, theoretical results of Fullerton *et al.* [12]; long-dashed line, theoretical results of Wöste *et al.* [17]; closed circles, experimental results of Hegemann *et al.* [15] and Hegemann [16].

By applying the density-matrix formalism of Blum [28] it is possible to relate the polarization fraction P'/P to the spin-specific amplitudes $f^{(2)}$ and $f^{(4)}$ as

$$\frac{P'}{P} = \left\{ \left(\frac{2}{3}|f^{(4)}|^2 + \frac{1}{3}|f^{(2)}|^2 \right) - 2\left(\frac{4}{27}|f^{(4)} - f^{(2)}|^2 \right) \right\} \left(\frac{d\sigma}{d\Omega} \right)^{-1}. \tag{29}$$

III. NUMERICAL PROCEDURE

The complex optical potential is derived from a fully molecular near-Hartree-Fock SCF wave function of the oxygen ground state. This wave function is calculated using the standard $[5s,4p]$ contracted basis of Dunning [29] augmented with one d function with exponent $\alpha = 0.9$ centered on the nuclei. At the experimental internuclear distance of $2.2874a_0$ the calculated total SCF energy is -149.6401 a.u., which compares well with the result of da Paixão *et al.* [10] (-149.6394 a.u.) and with the Hartree-Fock limit [30] (-149.6659 a.u.). The partial-wave expansion of all bound orbitals and of the static potential was truncated at $l_p = 40$. With this truncation parameter, the normalizations obtained for the bound orbitals were better than 0.999. In order to ensure convergence of the scattering solutions, terms up to $l_p = 20$ and $m_p = 17$ were included for all angular-momentum expansions. The radial integrations were performed over a grid containing 650 points, extending from the origin to 119.6 a.u. Three iterations of the SVIM provided converged solutions for all channels.
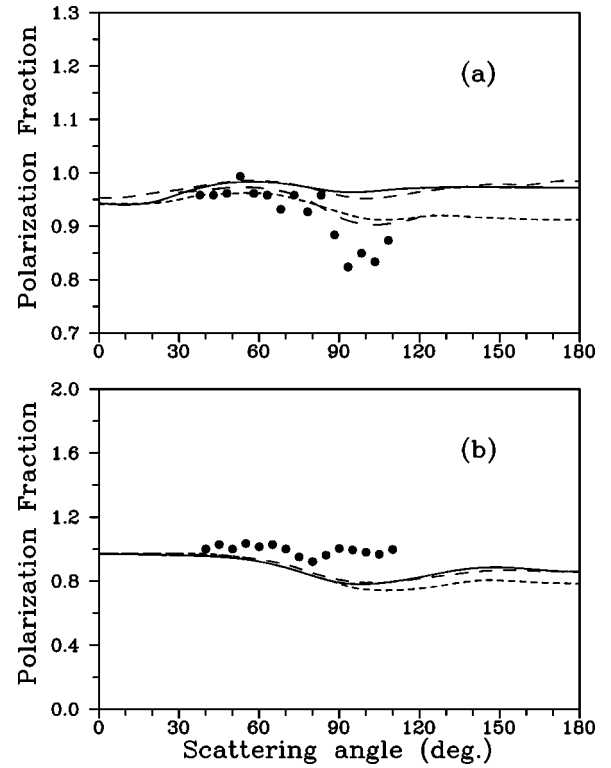

FIG. 10. Same as Fig. [9], but for (a) 10 eV and (b) 15 eV, except: short-dashed line, theoretical results of da Paixão *et al.* [10].

IV. RESULTS AND DISCUSSION

In Figs. 1–6 and in Tables I and II we show our calculated DCSs for elastic e^--O_2 scattering at incident energies (E_0) ranging from 5 to 500 eV, along with some available experimental and theoretical results. For energies below 50 eV, the absorption effects are small and thus can be neglected. In general, a very good agreement between our results and the experimental data is observed. Below 10 eV, our calculations were able to predict the structures in the DCS at small scattering angles shown in the experimental data of Sullivan *et al.* [9]. At 10 and 15 eV, our results are in good agreement with the SMC results of da Paixão *et al.* [10] and the nine-state R-matrix DCSs of Nordbeck *et al.* [13] mainly for scattering angles $\theta \lesssim 120°$. For energies above 15 eV, there are no other theoretical DCSs reported in the literature; therefore, comparisons were made only with the experimental data. At 20 eV, our calculations were able to provide DCSs in good agreement with the experimental data. At 50 and 100 eV, the calculated results are in very good qualitative agreement with the measured data of Shyn and Sharp [2]. Quantitatively, our results lie above the measured DCSs at intermediate and large scattering angles. For these energies, the inclusion of the absorption effects introduced only small improvement in the calculated DCSs, as can be seen in Figs. 4(b) and 5(a). On the other hand, at $E_0 = 200$ eV the absorption effects are shown to be significant; their inclusion in our calculations led to an excellent agreement with the measured data of Daimon *et al.* [5], as can be seen in Fig. 5(b). For $E_0 > 200$ eV our DCSs, calculated both with and without the inclusion of absorption effects, are in very good agreement with the measured data of Daimon *et al.* [5], Iga *et al.* [3], and Bromberg [4]. Nevertheless, the DCSs calcu-

lated with absorption effects are in better agreement with the measured data, except at large scattering angles. It is interesting to note that at 200 eV the experimental results of Shyn and Sharp lie systematically below those of Daimon *et al.* [5]. This discrepancy may suggest that the measured data of Shyn and Sharp could also be too low at 50 and 100 eV.

In Figs. 7(a) and 7(b) we compare our calculated ICSs and momentum transfer cross sections (MTCSs), respectively, with the available experimental and theoretical data. In general, our calculated results are in very good qualitative agreement with the measured data. Quantitatively, our cross sections lie within the experimental uncertainties, quoted as about 20%. Particularly, at higher incident energies, our results agree very well with those of Iga *et al.* [3] and Kanik *et al.* [7]. In addition, both our calculated ICSs and MTCSs exhibit a resonant structure at around 15 eV. In order to understand the physical origin of these resonances, calculations of partial-channel ICSs were carried out in the (5–50)-eV energy range, whose results are shown in Figs. 8(a) and 8(b) for the doublet and the quartet couplings, respectively. As can be seen, the enhancement of the cross sections at around 15 eV can be associated with both the $^2\Sigma_u^-$ and the $^4\Sigma_u^-$ resonances. In contrast to the prediction of Fullerton *et al.* [12], no resonance in the $^2\Pi_u$ scattering channel around 8 eV was found.

Figures 9 and 10 show our results of the polarization fraction P'/P for randomly oriented targets at energies $E_0 = 5, 8, 10,$ and 15 eV. Again, both experimental and other theoretical results available in the literature are shown for comparison. A good agreement can be observed between our results

and the theoretical results of da Paixão *et al.* [10], Fullerton *et al.* [12], and Wöste *et al.* [17]. At 5 eV, the calculated P'/P of Wöste *et al.* [17] are essentially identical to those of Fullerton *et al.* [12] and therefore are not shown. The comparison with the experimental data of Hegemann *et al.* [15] and of Hegemann [16] is only reasonable. Our calculated P'/P for randomly oriented targets in the (20–50)-eV range (not shown) are essentially close to unity for all scattering angles. Unfortunately, neither experimental nor other theoretical results are available for these energies.

In summary, we have reported elastic DCSs, ICSs, and MTCSs for electron-O_2 collisions in the (5–500)-eV energy range, as well as the P'/P ratios in the (5–50)-eV range. A complex optical potential, derived from a fully molecular near-Hartree-Fock self-consistent-field wave function, was used to describe the electron-molecule interaction. Our calculations have shown that the correlation-polarization potential is very important at low incident energies whereas the influence of absorption effects is significant for intermediate energies (100–300 eV). In general, our calculated cross sections are in good agreement with the available experimental data and with other theoretical results. In addition, the observed enhancement in the ICSs and MTCSs at around 15 eV was identified as a resonance in the $^2\Sigma_u^-$ and the $^4\Sigma_u^-$ scattering channels.

ACKNOWLEDGMENTS

[1] S. Trajmar, D. C. Cartwright, and W. Williams, Phys. Rev. A **4**, 1482 (1971).

[2] T. W. Shyn and W. E. Sharp, Phys. Rev. A **26**, 1369 (1982).

[3] I. Iga, M.-T. Lee, J. C. Nogueira, and R. S. Barbieri, J. Phys. B **20**, 1095 (1987).

[4] J. P. Bromberg, J. Chem. Phys. **60**, 1771 (1974).

[5] H. Daimon, S. Hayashi, T. Kondow, and K. Kuchitsu, J. Phys. Soc. Jpn. **51**, 2641 (1982).

[6] Y. Itikawa, A. Ichamura, K. Onda, K. Sakimoto, K. Takayanagi, Y. Hatano, M. Hayashi, H. Nishimura, and S. Tsurubuchi, J. Phys. Chem. Ref. Data **18**, 23 (1989).

[7] I. Kanik, S. Trajmar, and J. C. Nickel, J. Geophys. Res. Planet **98** (E4), 7447 (1993).

[8] G. Wöste, C. J. Noble, K. Higgins, P. G. Burke, M. J. Brunger, P. J. O. Teubner, and A. G. Middleton, J. Phys. B **28**, 4141 (1995).

[9] J. P. Sullivan, J. G. Gibson, R. J. Gulley, and S. J. Buckman, J. Phys. B **28**, 4319 (1995).

[10] F. J. da Paixão, M. A. P. Lima, and V. McKoy, Phys. Rev. Lett. **68**, 1698 (1992).

[11] C. J. Noble and P. G. Burke, Phys. Rev. Lett. **68**, 2011 (1992).

[12] C. M. Fullerton, G. Woeste, D. G. Thompson, K. Blum, and C. J. Noble, J. Phys. B **27**, 185 (1994).

[13] R. P. Nordbeck, C. M. Fullerton, G. Woeste, D. G. Thompson, and K. Blum, J. Phys. B **27**, 5375 (1994).

[14] J. M. Ratliff, G. H. Rutherford, F. B. Dunning, and G. K. Walters, Phys. Rev. A **39**, 5584 (1989).

[15] T. Hegemann, M. Oberste-Vorth, R. Vogst, and G. F. Hanne, Phys. Rev. Lett. **66**, 2968 (1991).

[16] T. Hegemann, Ph.D. thesis, University of Münster, Germany, 1993 (unpublished).

[17] G. Wöste, K. Higgins, P. Duddy, C. M. Fullerton, and D. G. Thompson, J. Phys. B **29**, 2553 (1996).

[18] R. R. Lucchese, G. Raseev, and V. McKoy, Phys. Rev. A **25**, 2572 (1982).

[19] M.-T. Lee and V. McKoy, Phys. Rev. A **28**, 697 (1983).

[20] M.-T. Lee and I. Iga, J. Phys. B **32**, 453 (1999).

[21] A. W. Fliflet and V. McKoy, Phys. Rev. A **21**, 1863 (1980).

[22] U. Fano and D. Dill, Phys. Rev. A **6**, 185 (1972).

[23] N. T. Padial and D. W. Norcross, Phys. Rev. A **29**, 1742 (1984).

[24] J. O. Hirschfelder, C. F. Curtis, and R. B. Bird, *Molecular Theory of Gases and Liquids* (Wiley, New York, 1964).

[25] G. Staszewska, D. W. Schwenka, and D. G. Truhlar, Phys. Rev. A **29**, 3078 (1984).

[26] A. Jain and K. L. Baluja, Phys. Rev. A **43**, 202 (1992).

[27] R. R. Lucchese, D. K. Watson, and V. McKoy, Phys. Rev. A **22**, 421 (1980).

[28] K. Blum, *Density Matrix Theory and Applications* (Plenum Press, New York, 1981).

[29] T. H. Dunning, Jr., Chem. Phys. **53**, 2823 (1970).

[30] P. E. Cade and A. C. Wahl, At. Data Nucl. Data Tables **13**, 339 (1974).